Nuclear Materials and Energy 48 (2026) 102201

Contents lists available at ScienceDirect

Nuclear Materials and Energy

journal homepage: www.elsevier.com/locate/nme

Optimization of functionally graded W/SS 316L coating for fusion applications

Ashwini Kumar Mishra *, Jarir Aktaa

Karlsruhe Institute of Technology (KIT), Institute for Applied Materials, Hermann-von-Helmholtz-Platz 1, 76344 Eggenstein-Leopoldshafen, Germany

A R T I C L E I N F O

Keywords:
Nuclear fusion
First Wall
Functionally graded material (FGM)
Finite element simulations
Plasma-facing components

A B S T R A C T

W coatings have applications as a protective layer over the structural steel of the International Thermonuclear Experimental Reactor (ITER) temporary First Wall. In this work, a finite element simulation study of W/SS 316L functionally graded material (FGM) coatings was performed to determine the coating's design parameters that reduce the thermal stress-discontinuity at the interface. Simulations considering only W coatings were performed initially to determine the ITER temporary First Wall equivalent thermal load conditions. Afterwards, the simulations of W/SS 316L FGM coatings were performed for varying the number of gradient interlayers while keeping the FGM thickness constant. Then, the FGM thickness was varied while keeping the number of gradient interlayers constant. In the simulations, the thermal load during the deposition and under the heat flux cycle of the ITER temporary First Wall were considered. Based on the simulation results, a 4-interlayer coating system with an FGM thickness of 0.8 mm between the top W coating and the steel substrate was recommended for the application.

1. Introduction

The First Wall structure of the nuclear fusion power plant is exposed to high heat flux cycles and neutron irradiation during operation. Recently, a tungsten (W) coating became a favourable material as a protective layer over the structural material of the First Wall due to its high thermal conductivity and melting point, as well as its low sputtering erosion and deuterium retention properties [1,2]. Therefore, W coatings are planned to be deposited over the structural material (steel) of the temporary First Wall of the International Thermonuclear Experimental Reactor (ITER) during the "Start of Research Operation" (SRO) phase [3].

Although W is a suitable material, its coefficient of thermal expansion (CTE) is much lower than that of steel [4,5]. Direct coating of W on steel develops high thermal stress discontinuity at the interface during the coating process and fusion operation, which can lead to delamination. This problem can be solved by a functionally graded material (FGM) layer between the top tungsten coating and the steel substrate. A similar approach was used for functionally graded W/EUROFER coatings for DEMO First Wall applications [6–10]. A systematic finite element (FE) simulation approach was implemented to determine the coating gradient parameters [11,12]. Low-pressure plasma-sprayed (LPPS) functionally graded W/EUROFER coatings were successfully deposited over small-scale to large-scale components [6–8].

Stainless steel (SS 316L) will be used as a structural material for the ITER temporary First Wall (TFW) [3]. Wang et al. [13] deposited W coatings on 316L steel substrate using the detonation spraying method and the atmospheric plasma spraying (APS) method. Klecka et al. [14] successfully deposited thick functionally graded W/316L coatings using the radio frequency inductively coupled plasma (RF-ICP) spray method. Three different volume fractions of W (25%, 50%, and 75%) were deposited. Heuer et al. [15] deposited functionally graded tungsten/steel coatings using a modified water-stabilized atmospheric plasma spraying method. The same three volume fractions of W (25%, 50%, and 75%) were deposited. Literature [13–15] shows the successful deposition of W and W/stainless steel FGM coatings, but without optimizing the gradient coating parameters (number of gradient interlayers and thickness). Dose et al. [16] determined the gradient parameters for W/AISI316L FGM with the help of analytical solution and the FE method. The thermal boundary conditions of the study were different from those of the ITER temporary First Wall, and the thermal load history of coatings during the deposition process was not considered. Finite element simulation studies of W/EUROFER FGM layers were performed in the literature [12,17,18]. SS 316L steel is planned to be used in ITER TFW,

* Corresponding author.
E-mail address: ashwini.mishra@kit.edu (A.K. Mishra).

https://doi.org/10.1016/j.nme.2026.102201
Received 6 May 2026; Received in revised form 26 July 2026; Accepted 4 August 2026
Available online 5 August 2026
2352-1791/© 2026 The Authors. Published by Elsevier Ltd. This is an open access article under the CC BY-NC-ND license (http://creativecommons.org/licenses/by-nc-nd/4.0/).

and the thermo-mechanical properties of EUROFER steel [11] are different from those of SS 316L steel [5], in particular, yield stress and CTE are quite different. Hence, simulation-based optimized gradient and thickness for W/EUROFER FGM cannot be directly applied for W/SS 316L FGM coatings.

Based on the current available literature, it can be interpreted that functionally graded W/SS 316L steel coatings can be deposited, but there is a need for a systematic study to determine the gradient coating parameters. The objective of this work is to perform finite element (FE) simulations to optimize the gradient parameters for functionally graded W/SS 316L coatings. Initially, the FE simulations were performed for only the W coating with varying heat flux cycles to determine an equivalent operation condition for the ITER temporary First Wall. Afterward, FE simulations were performed for a functionally graded W/SS 316L coating system with constant FGM layer thicknesses and varying the number of gradient interlayers. A thermal load during the coating deposition and heat flux cycles was simulated. The best-suited number of gradient interlayers was determined based on finite element (FE) simulations. Then FE simulations were performed for a fixed number of gradient interlayers and varying the FGM thicknesses to optimize the feasible FGM thickness. Hence, the most suitable W/SS 316L coating system among all other coating systems considered was determined based on a comparison of FE simulation key results.

2. Method

The FE simulations of functionally graded W/SS 316L coatings on SS 316L steel substrate, performed to optimize the gradient interlayer and their thickness, were conducted using Abaqus/CAE 2022 software. The coated ITER Temporary First Wall (TFW) components are large plates, modelled in the simulations by a two-dimensional section (ABCD), as shown in Fig. 1a.

The boundary conditions were applied to the coated two-dimensional section, so that it was equivalent to any section within a large unconstrained plate except for those at its edges. Thereby, a symmetric boundary condition was implemented to the left edge (AB) of the coated section model, and a kinematic coupling constraint was applied to its right edge (CD). The coupling constraint restricts the edge effect and allows the edge CD to deform (translation and rotation), while remaining straight. The movement of the lower-left side point (B) was restricted in the y-direction. The FE mesh of the coated section model was then generated using 4-node coupled-temperature-displacement generalised plane strain mesh elements (CPEG4T). These mesh elements are suitable for heat transfer and stress analysis in the same model, and generalised plane strain elements for simulating a section of a large unconstrained plate. A very refined mesh size of ≈ 6 μm x 6 μm was used in the top W coating and FGM layer. A mesh sensitivity analysis was performed by simulating various mesh sizes for a 3+2 interlayer coating system, since this system had the smallest interlayer thickness, as shown in Fig. S.1 of supplementary data. A maximum compressive thermal stress in the top W coating and stress-discontinuity ($|\Delta\sigma_{11}|$) at the interface 2 (FGM/SS 316L) for a 3+2 interlayer coating system, at 100 s of heat flux cycle, were utilized as the mesh sensitivity parameters. Simulations were performed for five mesh sizes: 4 μm, 6 μm, 7.5 μm, 10 μm, and 30 μm. The relative change in the maximum compressive stress in W and the stress discontinuity at the interface 2 (FGM/SS 316L) at 100 s from mesh size 30 μm to 4 μm was less than 0.2% and 0.01%, respectively. Overall, the effect of mesh size was low. A mesh size of 6 μm was selected for simulations.

The thickness of the top tungsten layer and the total coated section thickness were 0.1 mm and 20.1 mm, respectively. The elastic-ideal plastic properties, coefficient of thermal expansion (CTE), and thermal

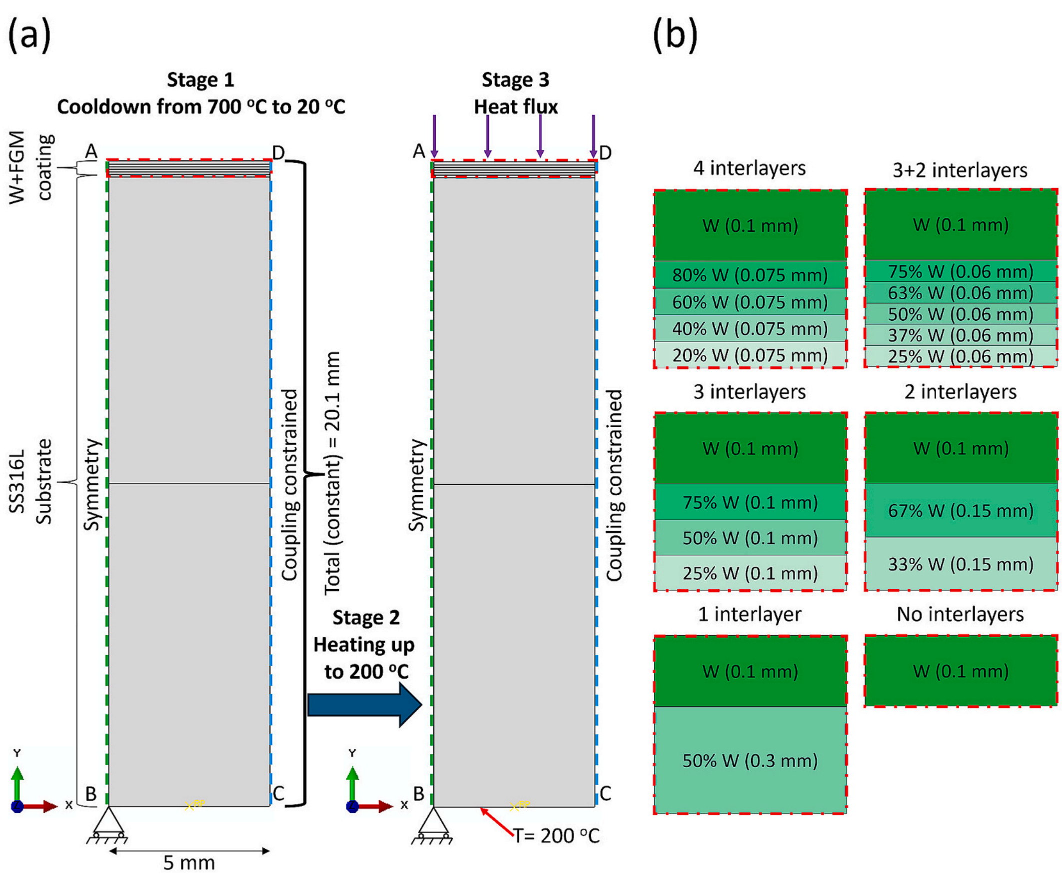

Fig. 1. a) FE model of W/SS 316L FGM coatings on SS 316L steel substrate with simulation stages, and b) schematic of varying number of interlayers in W/SS 316L FGM coatings

conductivity of SS 316L [5] and W [4,11,19] were used in the FE model as given in Table 1 and Table 2, respectively. Table 1 and Table 2 include the properties at a representative temperature. Yield stress data of SS 316L were obtained for an extended range of temperature by fitting the correlation of data from the reference [5] between 20 °C and 550 °C. The fitted correlation was then used to extrapolate linearly to the data beyond 550 °C. Similarly, the yield stress data of W were obtained for an extended range of temperature by fitting the correlation of data from the reference [11]. The properties of the gradient interlayers were determined by using the mixing rule, which considers the volume fraction of W and SS 316L. The mixing rule for FGM properties was based on the literature [20–22]. The effect of the coating's microstructure (porosity and lamellar splat structure) was not considered in the simulation. Heuer et al. [18] have compared the maximum stress and strain of the W/EUROFER FGM component after cooling to room temperature using FG layer properties determined by the ideal rule of mixture and actual measured material properties. The difference between actual measured material and the ideal rule of mixture properties models for the maximum von Mises stress and maximum local plastic strain was nearly 13% and -20%, respectively. This shows that a rule of mixture is a reasonable assumption for FGM materials.

FE simulations were performed in three thermal load stages. In the first stage, the whole coated section model was cooled down from 700 °C (initial stress-free state) to 20 °C. This stage simulates the thermal residual stress developed during the deposition due to the CTE mismatch between the different layers. With the initial stress-free state at 700°C, it is assumed that the substrate is homogenously heated during the coating process, e.g., LPPS, to 700 °C which is considered as the maximum steel substrate temperature to avoid the formation of intermetallic precipitates [15]. In the second stage, the whole coated section model was heated to 200 °C. In the third stage, five heat-flux cycles were used as thermal load to the top surface of the W top layer (AD). The applied heat flux cycles were the ITER temporary First Wall equivalent conditions, determined in this work (section 3.1). Each cycle had a 10 s of heating phase and 10 s of cooling phase. In the heating phase, the heat flux was applied for 2 s and subsequently kept constant for 8 s. Similarly, the heat flux was removed in 2 s and followed by further cooling for 8 s. A boundary condition of uniform temperature (200 °C) was applied on the bottom surface of the model (BC) as shown in Fig. 1a. These three thermal load stages were applied in the FE simulation using two steps. Stages 1 and 2 were applied to the whole coated section model, so they were combined in the first step of the FE simulation. The third stage was applied in the second step of the FE simulation.

Three sets of simulations were performed. 1st set of simulations was performed to determine the heat-flux cycle that can be applied to the coated section as an equivalent condition for the ITER temporary First wall. Therefore, a coated section with 0.1 mm of W layer over a 20 mm steel substrate was considered. With this coated section, four FE simulations were performed with the same 1st step, but in the second step, a different maximum heat-flux cycle was applied. Four different maximum heat fluxes of 0.25, 0.28, 0.3, and 0.4 MW/m^2 were considered in the four FE simulations, as shown in Fig. 2a. The maximum planned surface temperature for the ITER Temporary First Wall (TFW) during the start of research operation (SRO) phase is 500 °C. Hence, the maximum heat flux, which yields a maximum surface temperature close to 500 °C was chosen for further study.

2nd set of simulations was performed with an FGM layer between the top W layer and the steel substrate. The number of interlayers was varied from 1 to 4, as shown in Fig. 1b. The total FGM layer thickness was 0.3 mm in all coating systems. The same 2 simulation steps were applied to all 5 coating systems. The simulation results with zero interlayers were obtained from the first set of simulations and compared with the coating system from the second set of simulations.

3rd set of simulations was performed with a 4-interlayers coating system, and varying the total thickness of the FGM layer such that the total thickness of the steel substrate and FGM layer was 20 mm. The thickness of the W coating was always fixed. Seven coating systems were simulated with FGM layer thicknesses of 0.4, 0.5, 0.6, 0.7, 0.8, 0.9, and 1.2 mm. The simulation results with zero interlayer and 4 interlayer coating system with FGM thickness of 0.3 mm were taken from the 1st and 2nd sets of simulations and compiled with those of the 3rd set of simulations.

In this work, any variation of parameters (maximum stress, stress-discontinuity, and maximum equivalent plastic strain (PEEQ)) less than 1% was considered identical. Such small variations may arise from FE simulations and are not significant.

Table 1
Material properties of SS 316L [5] steel used in FEM simulations

Temperature	Young's modulus	Poisson's ratio	Yield stress	Thermal conductivity	CTE
°C	GPa	-	MPa	W/(m.K)	10^{-6}/K
20	200	0.3	190	14.28	15.30
100	193	0.3	165	15.48	15.90
200	185	0.3	137	16.98	16.60
300	176	0.3	119	18.49	17.20
400	168	0.3	107	19.99	17.80
500	159	0.3	99	21.49	18.30
600	151	0.3	96	22.99	18.70
700	142	0.3	93	24.49	19.00

Table 2
Material properties of W [4,11,19] used in FEM simulations.

Temperature	Young's modulus	Poisson's ratio	Yield stress	Thermal conductivity	CTE
°C	GPa	-	MPa	W/(m.K)	10^{-6}/K
20	396	0.280	1360	51.14	4.40
100	395	0.281	1266	48.52	4.41
200	394	0.281	1155	46.22	4.42
300	392	0.282	1049	46.10	4.44
400	389	0.283	948	47.27	4.46
500	386	0.284	854	48.84	4.49
600	383	0.285	765	50.20	4.52
700	378	0.287	681	52.62	4.56

3. Results and discussion

3.1. Optimizing the heat flux cycle for the ITER Temporary First Wall

Fig. 2a shows the heat-flux cycles applied to four coating systems of 1st set of simulations. The temperature on the top surface of the coated section (from node A) is shown in Fig. 2b. In all four coating systems, the minimum temperature was the same during the cooling phase, while the maximum temperature during the heating phase increased with heat flux. The coated section with the maximum heat flux of 0.28 MW/m^2 had a maximum surface temperature close to 500 °C, which was the maximum planned surface temperature for the ITER Temporary First Wall (TFW) during the start of research operation (SRO) phase. So, the heat-flux cycle with the maximum heat flux of 0.28 MW/m^2 was considered as the Temporary First Wall equivalent condition and used in the further 2nd and 3rd sets of simulations.

It should be noted that the actual heat-flux value in the ITER Temporary First Wall (TFW) can vary according to the thermal boundary conditions, but the maximum and minimum temperatures of the thermal cycle will be similar. In this work, all FGM coating systems were subjected to the same applied heat-flux cycle and compared to optimize the number of gradient interlayers and thickness. A similar approach was used in the literature [17,23].

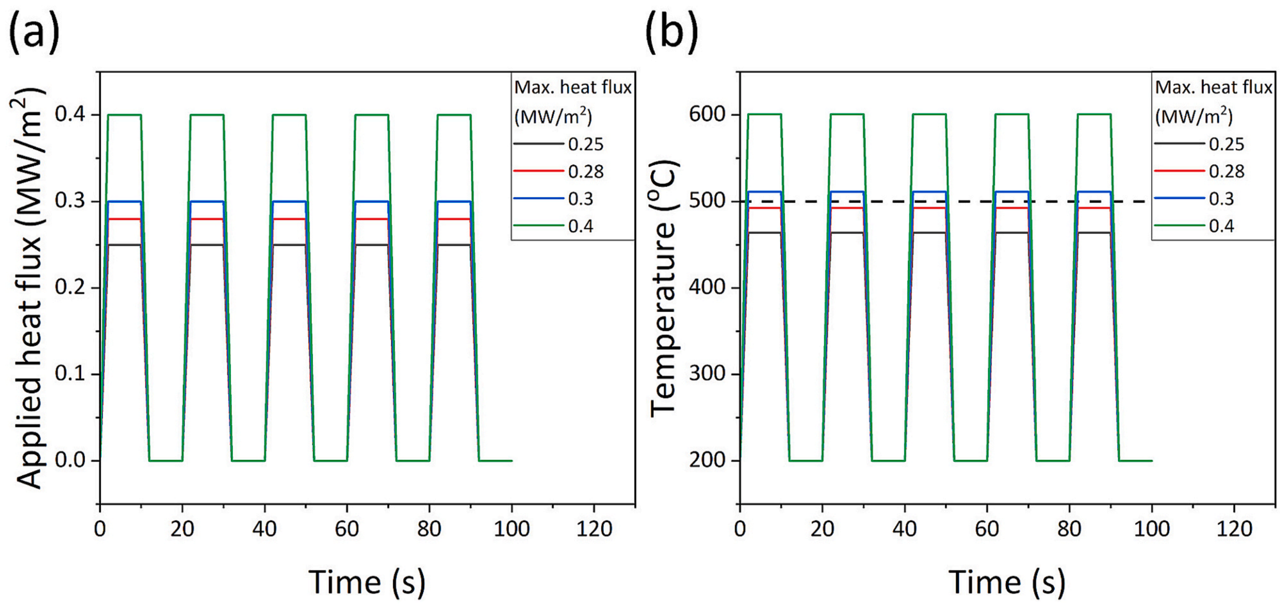

Fig. 2. a) Applied heat flux cycles on four coating systems of 1st set of simulations, and b) temperature on the top surface of the coated section for four coating systems.

3.2. Optimizing the number of gradient interlayers

Fig. 3 a-e) shows the thermal residual stress (σ_{11}) across the cross-section of the coated section (along AB as shown in Fig. 1a) after coating deposition (stage 1 of simulations). These simulations considered thermal residual stress developed due to the coefficient of thermal expansion mismatch between the different layers. The other components of the residual stresses (quenching stress) were not considered because they are not affected by the gradient. The objective was to design a gradient layer to solve the problem of the coefficient of thermal expansion mismatch. So, simulating only thermal residual stress was sufficient. This residual stress was used for comparison of various coating systems and determining the most suitable system. A similar approach was used in the literature [21,22,24] to determine the residual stress of coatings.

In all coating systems, the top W coating was under a high compressive stress, and the steel substrate near the interface was under tension. A large discrete stress drop was found at the coating/substrate interface in the 0 interlayer system due to the large CTE mismatch between W and steel. The thermal residual stress decreases more gradually from the top W layer to the substrate with an increased number of interlayers. The large discrete stress drop was reduced with the increasing number of interlayers. This was the benefit of the FGM layer between the top W layer and the steel substrate. A maximum compressive stress in the top W coating was not influenced by the number of interlayers. A similar observation was found in the literature for the other FGM system [25] determined using an analytical model. A reduction in the discrete stress drop at the interface may reduce the interface cracking. The maximum tensile stress in the steel substrate increased from 0 interlayer coating system to 1 interlayer coating system. While it remained the same from 1 interlayer to 4 interlayer coating systems. The overall thickness of the steel substrate and FGM layer was kept constant (= 20 mm) in all simulations. The steel substrate thicknesses for 0 layer system and the FGM coating system were 20 mm and 19.7 mm, respectively. So, the maximum tensile stress in the steel substrate depends on the steel thickness but not on the number of gradient interlayers. For a better comparison, the discrete stress drop (stress-discontinuity ($|\Delta\sigma_{11}|$)) was measured and plotted in Fig. 3f.

Fig. 3f shows the stress-discontinuity ($|\Delta\sigma_{11}|$) at two interfaces for varying number of interlayers. In this work, stress-discontinuity was measured as an absolute value. The interface between the W and FGM layer is named as interface 1, while the interface between the FGM layer and the steel substrate is named as interface 2. W/FGM interface in the 0 interlayer coating system was the interface between W and the steel substrate. The stress-discontinuity at interface 1 decreased as the number of interlayers increased from 0 to 4. Similarly, the stress-discontinuity decreased at interface 2 as the number of interlayers increased. For a 3 interlayer and 3+2 interlayer system, the stress discontinuity was the same at both interfaces (1 and 2). The advantage of the 3+2 interlayer system was to decrease the stress discontinuity within the FGM layer (between the 75 % W and 25% W layers), as shown in Fig. 3d.

The maximum PEEQ for the 0 interlayer system was 4% higher than the other coating systems with an FGM layer. There was no effect of the increased number of interlayers on the maximum PEEQ for 1 to 4-interlayer coating systems.

Fig. 4a shows the ITER Temporary First Wall (TFW) equivalent heat-flux cycle, with the maximum heat flux of 0.28 MW/m^2 used in the 2nd and 3rd sets of simulations. Fig. 4b and c show the thermal stress (σ_{11}) during the heat flux cycle at 90 s and 100 s, respectively. At 90 s, the coating system is in the heating phase, and at 100 s, in the cooling phase of the heat flux cycle. The top W coating was under tensile stress at 90 s while under compression at 100 s. The stress condition was alternating because of the temperature cycle generated by the applied heat-flux cycles. At both times (90 s and 100 s), the thermal stress gradually changes with increasing number of interlayers. The maximum tensile stress in the W coating at 90 s was nearly the same for all coating systems. The maximum compressive stress in the W coating at 100 s decreased from 0 to 1 interlayer coating system. Afterwards, it was nearly constant for all FGM coating systems (1 to 4 interlayers).

Fig. 4d shows the stress-discontinuity ($|\Delta\sigma_{11}|$) at two interfaces. The stress-discontinuity ($|\Delta\sigma_{11}|$) at 90 s at interface 1 decreased with increasing interlayer numbers. At interface 2, stress-discontinuity increased with the number of interlayers, although the magnitude of a 4 interlayer system was lower than that of the other conditions. The stress discontinuity for the 3 interlayer coating system was nearly the same for the 3+2 interlayer coating system at interfaces 1 and 2.

Furthermore, the stress-discontinuity at 100 s for interfaces 1 and 2 decreased with increased interlayer numbers. The stress discontinuity for the 3+2 interlayer coating system was slightly higher than that of the

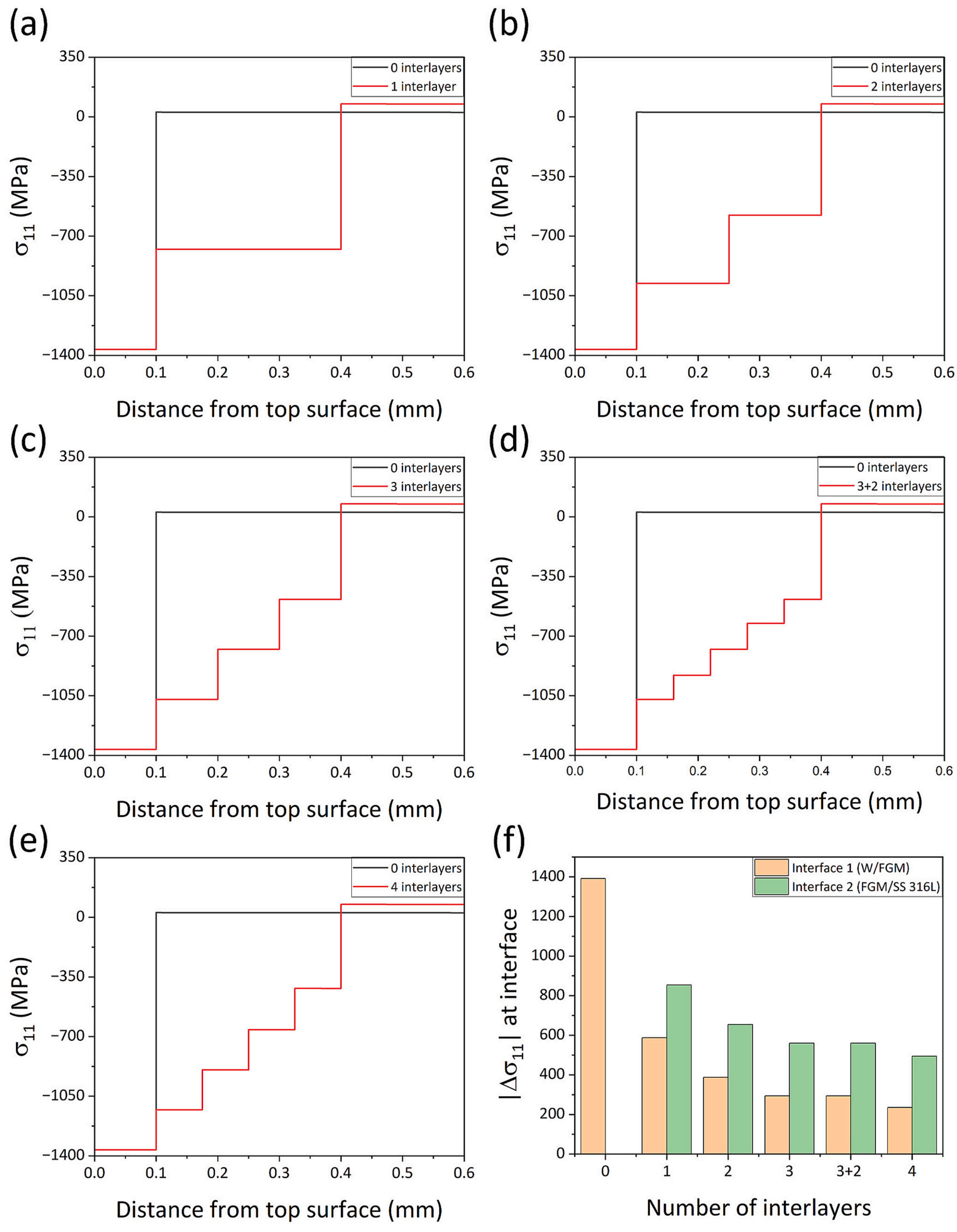

Fig. 3. Thermal residual stress (σ_{11}) after coating deposition for a) 1 interlayer, b) 2 interlayers, c) 3 interlayers, d) 3+2 interlayers, e) 4 interlayers system in comparison with 0 interlayers system, and f) stress-discontinuity ($|\Delta\sigma_{11}|$) at the interface versus number of interlayers in the coating system after coating deposition

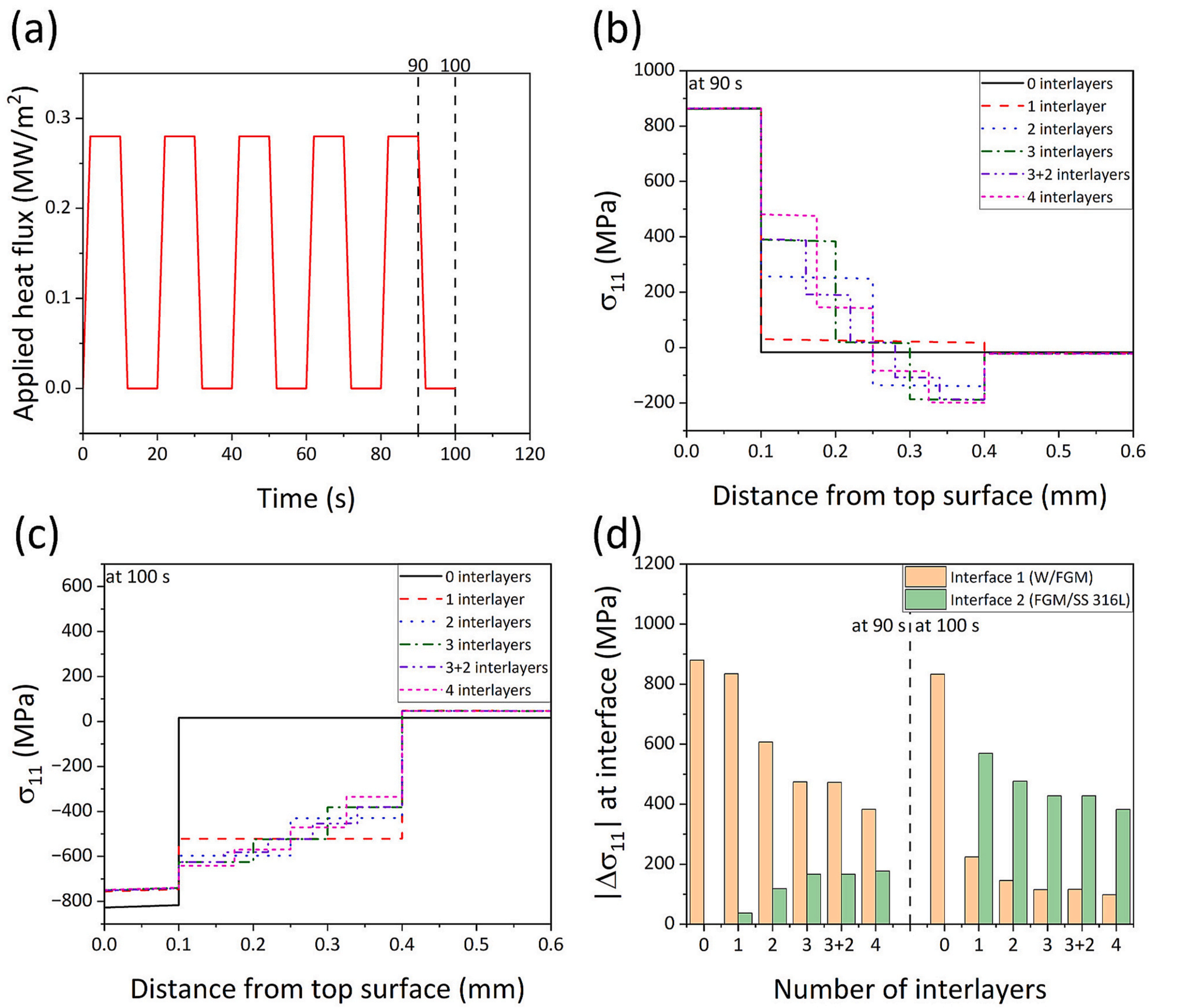

Fig. 4. a) Heat-flux cycles with the maximum heat flux of 0.28 MW/m^2 used in the 2nd and 3rd sets of simulations. Thermal stress (σ_{11}) during heat flux cycle at b) 90 s, c) 100 s. d) Stress-discontinuity ($|\Delta\sigma_{11}|$) at the interface for a varying number of interlayers in the coating system

3 interlayer coating system at interface 1, while the values were the same at interface 2.

The effect of the number of interlayers on maximum PEEQ after 100 s of heat flux cycle was the same as after the deposition condition. Maximum PEEQ was highest for the 0 interlayer system. While it was nearly the same for all FGM coating systems (1 to 4 interlayers).

The number of interlayers in the FGM coating system doesn't have a significant effect on the maximum stress in the top W coating. Based on the stress analysis (after deposition and during heat-flux cycle conditions), a 4-interlayer system was the best among the other simulated coating systems for reducing the thermal stress discontinuity at the interface.

3.3. Optimizing the thickness of the gradient layer

A 4-interlayer system was found to be most suitable for the temporary First Wall conditions. Afterwards, simulations were compared for nine coating systems with a 4-interlayers and varying FGM thicknesses of 0, 0.3, 0.4, 0.5, 0.6, 0.7, 0.8, 0.9, and 1.2 mm. Fig. 5a, b, and c show the thermal residual stress contour after coating deposition for 3 systems with FGM layer thicknesses of 0, 0.8, and 1.2 mm, respectively. The maximum compressive stress in the top W coating was not affected by an increased FGM thickness. Stress from the top tungsten layer to the steel substrate changes more gradually from compressive to tensile with increasing FGM thickness.

Fig. 6a shows the stress-discontinuity ($|\Delta\sigma_{11}|$) at the interface with increasing FGM thickness for a 4-interlayer system after coating deposition. Stress discontinuity at interface 1 decreased from 0 interlayer ($t_{FGM} = 0$ mm) to 4 interlayer ($t_{FGM} = 0.3$ mm) systems, while there was no change in stress discontinuity with increasing FGM thickness for a 4-interlayer system. Stress discontinuity at interface 2 decreases with increasing FGM thickness.

Fig. 6b shows the maximum compressive stress in the top W tungsten coating and the maximum tensile stress in the steel substrate after coating deposition. The maximum compressive stress in the top W coating was the same for all coating systems. The maximum tensile stress in the steel substrate increased with increasing FGM thickness. The increased tensile stress can lead to undesirable plastic deformation of the steel substrate. For further analysis, the maximum equivalent plastic strain (PEEQ) of the top W coating and SS 316L steel substrate with increasing FGM thickness for a 4-interlayer system after coating deposition was plotted in Fig. 6c.

The maximum PEEQ in the top W coating decreased with increasing the FGM thickness. The maximum PEEQ in the steel substrate was zero

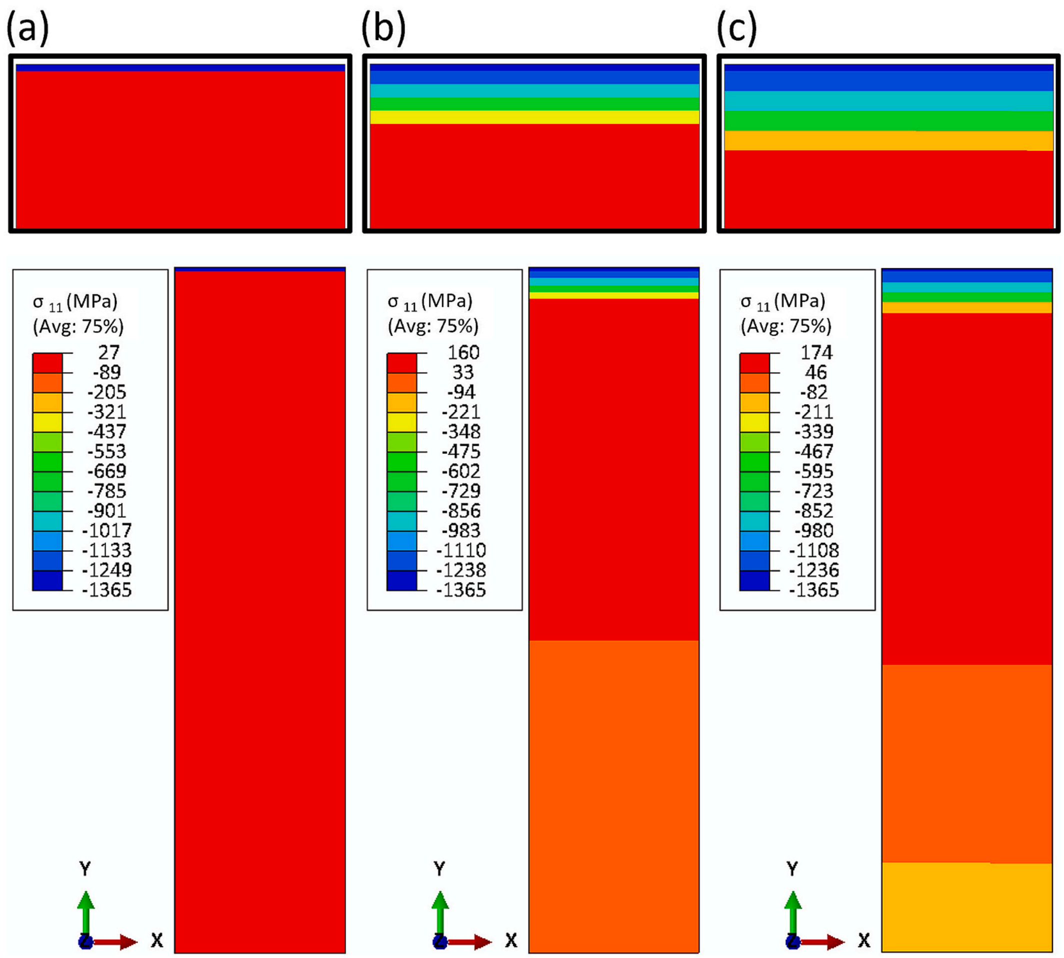

Fig. 5. Thermal residual stress (σ_{11}) after coating deposition for a 4-interlayer system with FGM thickness of a) 0 mm, b) 0.8 mm, and c) 1.2 mm

up to an FGM thickness of 0.7 mm and negligible for an FGM thickness of 0.8 mm. The Maximum PEEQ in the steel substrate started increasing beyond the FGM thickness of 0.8 mm. Decreasing the PEEQ in the top W coating was beneficial, but beyond a certain FGM thickness, at the cost of plastic deformation of the steel substrate. So, a maximum FGM thickness of 0.8 mm can be deposited without a significant deformation of the steel substrate.

Fig. 7a and b show the thermal stress during the heat-flux cycle at 90 s and 100 s, respectively. The maximum tensile stress at 90 s and the maximum compressive stress at 100 s in the top W coating layer varied with the FGM thickness. Fig. 7c and d show the stress-discontinuity ($|\Delta\sigma_{11}|$) at the interface at 90 s and 100 s with increasing FGM thickness for a 4-interlayer coating system. The stress discontinuity at the interface 1 at 90 s decreased from 0 to 0.3 mm FGM thickness. Afterwards, the stress discontinuity varies non-monotonously with varying the thickness from 0.3 mm to 1.2 mm, while the overall variation was low (less than 11.5%). The stress discontinuity at interface 2 at 90 s was nearly the same (variation less than 2%) for the FGM thickness variation from 0.3 mm to 0.8 mm; afterwards, it decreased up to a thickness of 1.2 mm.

The stress discontinuity at interface 1 at 100 s decreased with increasing FGM thickness up to an FGM thickness of 0.5 mm. Afterwards, the stress discontinuity increases with increasing FGM thickness from 0.5 mm to 1.2 mm. For interface 2, the stress discontinuity decreases monotonously with increasing FGM thickness.

The stress-discontinuity parameters of both interfaces at 90 s and 100 s were inconclusive for determining optimal thickness. The stress-discontinuity ($|\Delta\sigma_{11}|$) at both interfaces and times (90 s and 100 s) depends on the maximum thermal stress in the top W coating and steel substrate. For a detailed understanding, Fig. 8a and b show the maximum stresses in the top W coating and steel substrate at 90 s and 100 s, respectively. At 90 s, the maximum tensile thermal stress in the top W coating was nearly the same for FGM thicknesses of 0.3, 0.4, and 0.5 mm, and afterwards it decreased with increasing FGM thickness from 0.5 mm to 1.2 mm, as shown in Fig. 8a. Decreasing tensile thermal stress in the top W coating is beneficial for reducing the possibility of vertical cracks. But the maximum FGM thickness possible is 0.8 mm without plastic deformation of the steel substrate. The maximum compressive stress in the steel substrate varies non-monotonously with increased FGM thickness.

At 100 s, the maximum compressive stress in the top W coating initially decreases with increased FGM thickness from 0 to 0.5 mm. After that, the maximum compressive stress increases. Based on this, a thickness of 0.5 mm would be the minimum point. Tensile stress promotes vertical crack propagation in the coating, while compressive stress resists it. At 90 s, the maximum tensile stress of the top W coating was decreasing with increasing FGM thickness, and a maximum thickness of 0.8 mm was possible without significant plastic deformation of the steel substrate. In order to have an advantage of reduction in tensile stress in the top W coating at 90 s, a thickness of 0.8 mm is more beneficial than reducing compressive stress at 100 s with FGM thickness of 0.5 mm. Fig. 8c shows the maximum equivalent plastic strain (PEEQ) of the top W coating layer and SS 316L steel with increasing FGM thickness for the 4-interlayer system at 100 s. The maximum PEEQ of the top W coating decreases with increasing FGM thickness. The plastic deformation of the steel substrate was negligible up to an FGM thickness

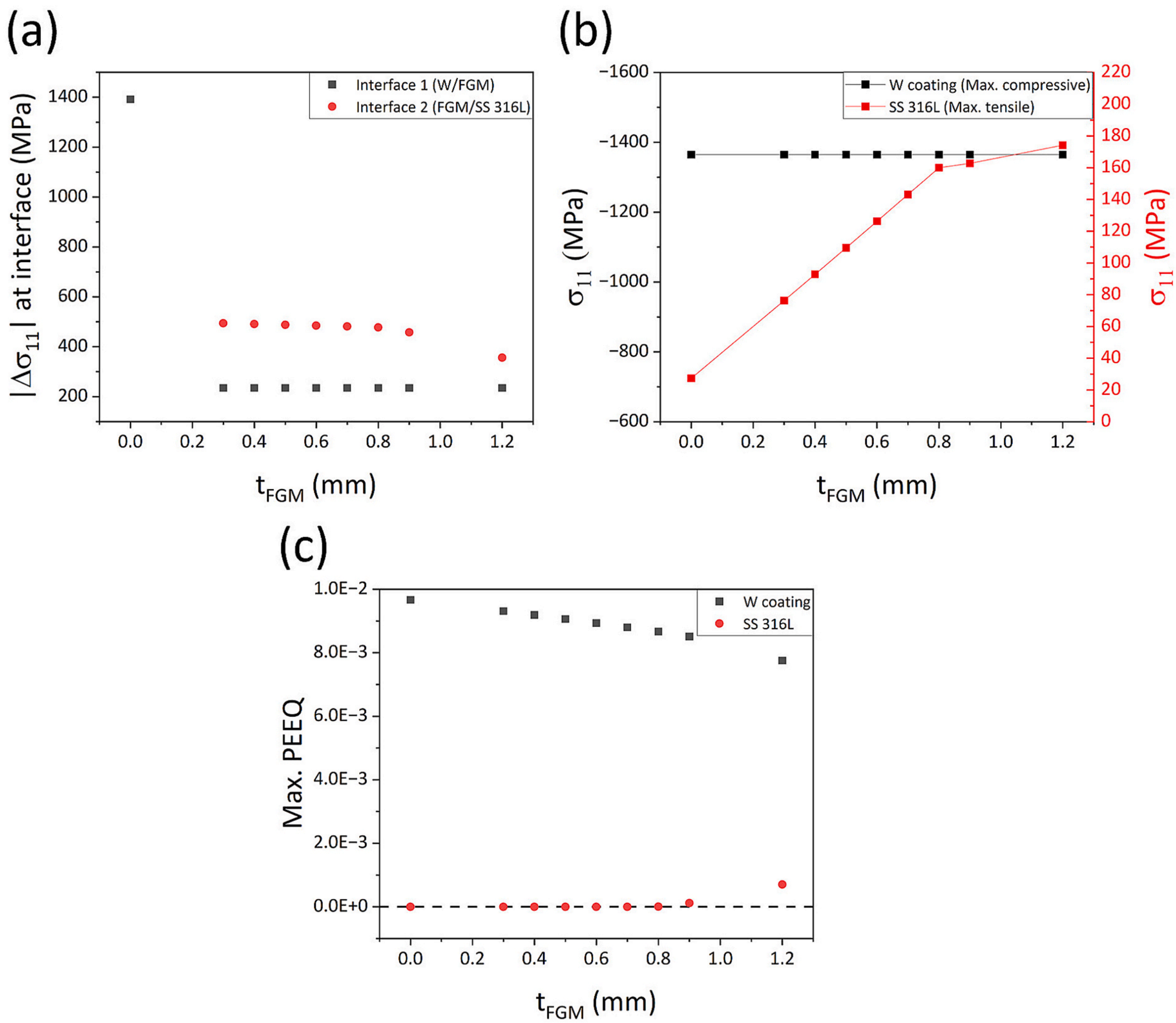

Fig. 6. a) Stress-discontinuity ($|\Delta\sigma_{11}|$) at the interface, b) maximum thermal stress and c) maximum equivalent plastic strain (PEEQ) of the top W coating and SS 316L steel substrate with increasing FGM thickness for a 4-interlayer system after coating deposition.

of 0.8 mm.

Overall, stress discontinuity at interface 2 after deposition decreases with increasing FGM thickness, the maximum PEEQ of the top W coating decreases with increasing FGM thickness after deposition and heat flux cycle (100 s), the maximum tensile thermal stress (at 90 s of heat flux cycle) in the top W coating decreases with increasing FGM thickness from 0.5 mm to 1.2 mm and plastic deformation of the steel substrate was negligible up to an FGM thickness of 0.8 mm after deposition and heat flux cycle (100 s). Based on these parameter analyses, a 4-interlayer coating system with an FGM thickness of 0.8 mm will be most suitable as a protective armour layer for the temporary First Wall of ITER.

The current work optimizes the W/SS 316L FGM coating parameters using a parametric variation approach. Initially, the number of interlayers was varied while keeping the FGM thicknesses constant; afterward, the number of interlayers was kept constant, and the FGM thickness was varied. The FGM interlayers result in a gradual stress decrease from the top W coating to the steel substrate, reducing the stress-discontinuity ($|\Delta\sigma_{11}|$) at the interface. Hence, FGM layers help in preventing delamination at the interface during deposition and under thermal cycles. A 4-interlayer FGM coating system was found to be most suitable as compared to other coating systems considered.

A similar observation was found in the case of W/EUROFER FGM coatings. Schmidtmann et al. [26] deposited approximately 450 μm of W coating directly over the EUROFER steel substrate without delamination, whereas approximately 800 μm of W coating was deposited with the W/EUROFER FGM layer in between successfully [6]. The use of W/EUROFER FGM coating results in successful coating of small-scale to large-scale First Wall size-relevant components [6–8].

Qu et al. [12] suggested an optimized thickness of 1.2 mm for W/EUROFER FGM coating. Heuer et al. [17] recommended the FGM thickness between 0.7 and 1.5 mm. The FGM parameters depend on the thermo-mechanical properties of the material. W/EUROFER FGM coating parameters cannot be directly implemented for W/SS 316L FGM coating. Also, the FGM thickness depends on the thermal load conditions and prescribed geometry parameters, e.g., top W coating thickness.

The choice of the correct evaluation parameter for optimization also affects the gradient coating parameters. Weber & Aktaa [11] and Dose et al. [16] designed the W/steel FGM interlayers without considering the stress-discontinuity ($|\Delta\sigma_{11}|$) at the interface as an optimization parameter. The key feature of the FGM design is to reduce the stress-discontinuity ($|\Delta\sigma_{11}|$) at the interface to increase the interface strength and thermal cycling life [24]. So, in this work, stress-discontinuity ($|\Delta\sigma_{11}|$) at the interface was considered as one of the optimization parameters. It is worth noting that the stress-discontinuity at the interface ($|\Delta\sigma_{11}|$) is not a direct measure of the quantitative interface fracture properties and thermal cycling life. These can be determined in the future on deposited W/SS 316L FGM coatings.

The current FEM work was performed based on preliminary

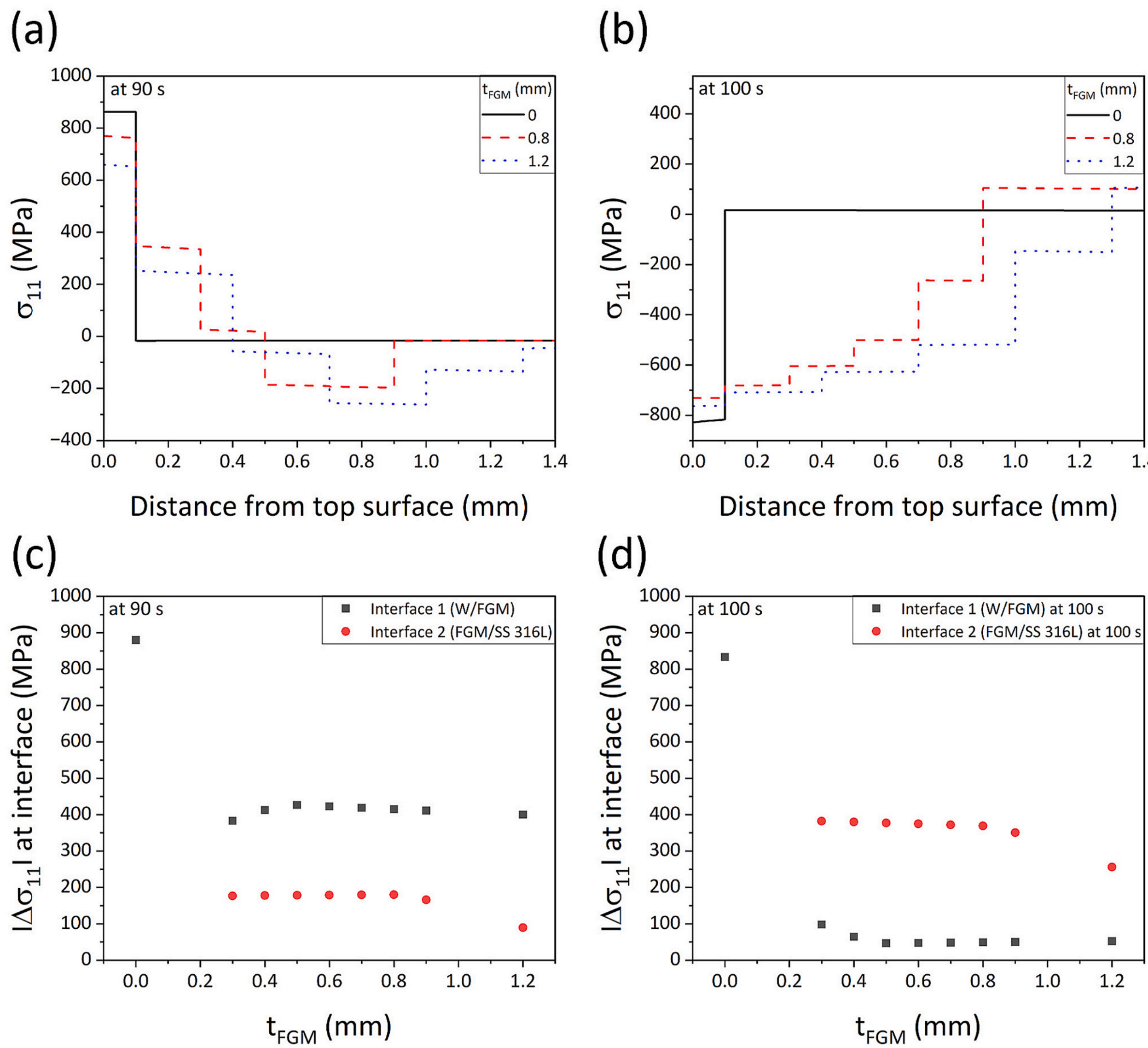

Fig. 7. Thermal stress (σ_{11}) during heat flux cycle at a) 90 s, and b) 100 s, stress-discontinuity ($|\Delta\sigma_{11}|$) at the interface at c) 90 s, and d) 100 s with increasing FGM thickness for 4-interlayer coating system

assumptions to assess the gradient parameter and save time and resources for actual W/SS 316L FGM coatings. These assumptions, such as a linear mixing rule for FGM interlayer properties without considering coating anisotropy and microstructure, as well as stress-free temperature, were chosen as the best estimation due to the lack of actual data. The thermal residual stress after coating deposition was determined assuming a uniform cooling of the whole coated section from stress-free temperature to room temperature without considering layer-by-layer deposition, particle impact during deposition, and coating microstructure (porosity or interface roughness). The interface between interlayers was assumed to be perfectly bonded without considering any fracture properties due to a lack of actual data. Hence, a deviation between the theoretical and actual stress-state is possible. In the future, W/SS 316L FGM coating's properties will be measured to help to further enhance simulations. Similarly, the effect of heating and cooling rate during the heat flux cycle was not incorporated due to the unavailability of data. In the current work, the simulation of five heat flux cycles was used to determine the best suitable coating system. However, fatigue, creep, irradiation effect, erosion, and long-term service life of the coating were not within the scope of the current study.

4. Conclusions and outlook

FE simulations of W/SS 316L FGM coating were performed in this work to determine the most suitable gradient coating parameters. The main conclusions of this work are as follows:

1. FE simulations of W coating over steel substrate performed under varying heat flux cycles resulted in a heat flux cycle with a maximum heat flux of 0.28 MW/m^2 as an ITER Temporary First Wall equivalent condition.
2. Based on the stress analyses of FE simulations of W/SS 316L FGM coating performed by varying the number of gradient interlayers, a 4-interlayer coating system was found to be the best among all other coating systems investigated for reducing the stress discontinuity at the interface.
3. Finite element simulations of W/SS 316L FGM coating performed on a gradient 4-interlayer coating system by varying the FGM layer thickness showed that an FGM layer thickness of 0.8 mm is suitable for reducing the tensile stress in the W coating during the heat flux cycle, without significant plastic deformation of the steel substrate.

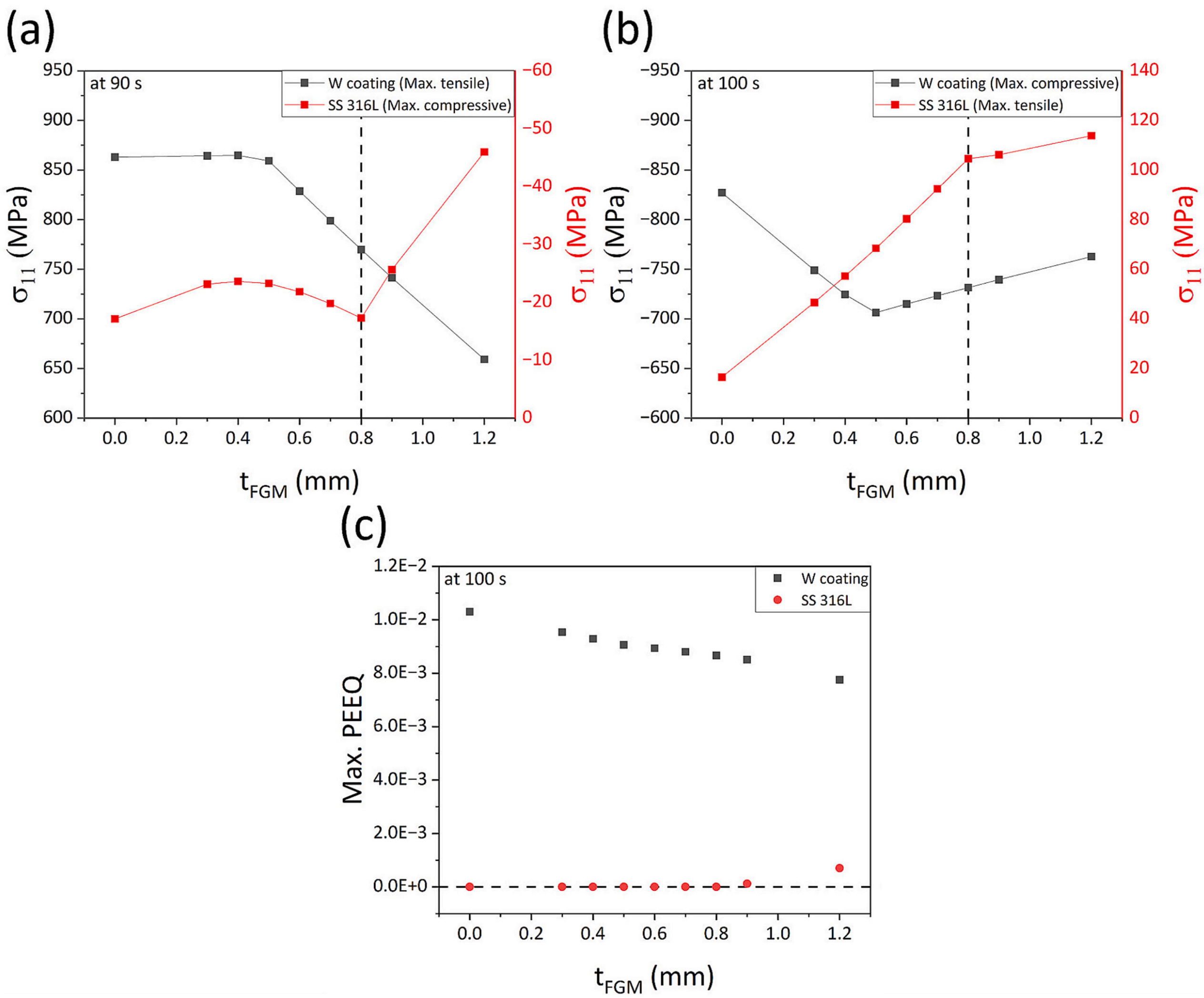

Fig. 8. Maximum thermal stress in the top W coating and SS 316L steel substrate at a) 90 s and b) 100 s, and c) maximum equivalent plastic strain (PEEQ) of the top W coating layer and SS 316L steel substrate (at 100 s) with increasing FGM thickness for a 4-interlayer system

Based on the results of this work, a 4-interlayer coating system with an FGM thickness of 0.8 mm was found to be most suitable among all other coating systems investigated for the ITER Temporary First Wall. Such functionally graded coatings can be deposited with the aforementioned, recommended coating parameters by thermal spraying, e.g., vacuum/low-pressure plasma spraying, which is planned as part of future work.

CRediT authorship contribution statement

Ashwini Kumar Mishra: Writing – review & editing, Writing – original draft, Visualization, Validation, Software, Methodology, Investigation, Formal analysis, Data curation, Conceptualization. **Jarir Aktaa:** Writing – review & editing, Supervision, Funding acquisition, Conceptualization.

Declaration of competing interest

The authors declare that they have no known competing financial interests or personal relationships that could have appeared to influence the work reported in this paper.

Acknowledgements

This work has been carried out within the framework of the EUROfusion Consortium, funded by the European Union via the Euratom Research and Training Programme (Grant Agreement No 101052200 — EUROfusion). Views and opinions expressed are however those of the author(s) only and do not necessarily reflect those of the European Union or the European Commission. Neither the European Union nor the European Commission can be held responsible for them.

Appendix A. Supplementary data

Supplementary data to this article can be found online at https://doi.org/10.1016/j.nme.2026.102201.

Data availability

Data will be made available on request.

References

[1] X. Yang, W. Qiu, L. Chen, J. Tang, Tungsten–potassium: a promising plasma-facing material, Tungsten 1 (2019) 141–158, https://doi.org/10.1007/s42864-019-00018-5.

[2] G. Schmidtmann, A. Litnovsky, A. Kreter, M. Rasinski, S. Möller, A. Houben, J. W. Coenen, R. Vaßen, S. Brezinsek, Ch. Linsmeier, O. Guillon, G. Mauer, Deuterium retention and erosion resistance of low-pressure plasma sprayed tungsten coatings, Journal of Nuclear Materials 619 (2026) 156267, https://doi.org/10.1016/j.jnucmat.2025.156267.

[3] F. Pesamosca, T. Ravensbergen, R.A. Pitts, D. Frattolillo, M. Erroi, Q. Deliege, P. C. de Vries, L. Zabeo, L. Pangione, I.S. Carvalho, A. Vu, Development of ITER first wall heat load feedback control, Nuclear Materials and Energy 41 (2024) 101781, https://doi.org/10.1016/j.nme.2024.101781.

[4] T. Nagasaka, R. Kasada, A. Kimura, Y. Ueda, T. Muroga, Theromophysical Properties and Microstructure of Plasma-Sprayed Tungsten Coating on Low Activation Materials, Fusion Science and Technology 56 (2009) 1053–1057. https://doi.org/10.13182/FST56-1053.

[5] AFCEN, Design and Construction Rules for Mechanical Components of Nuclear Installations (RCC-MRx), ISBN: 2-913638-57-6, Edition with first Addendum 2013, 2012.

[6] T. Grammes, T. Emmerich, J. Aktaa, W/EUROFER functionally graded coatings for plasma facing components: Technology transfer to industry and upscaling, Fusion Engineering and Design 173 (2021) 112940, https://doi.org/10.1016/j.fusengdes.2021.112940.

[7] T. Grammes, T. Emmerich, D. Qu, O. Heinze, R. Vaßen, J. Aktaa, Functionally graded tungsten/EUROFER coating for DEMO first wall: From laboratory to industrial production, Fusion Engineering and Design 188 (2023) 113430, https://doi.org/10.1016/j.fusengdes.2023.113430.

[8] T. Grammes, A.K. Mishra, K. Battalov, A. Purwitasari, T. Emmerich, J. Aktaa, Mechanical properties and quality of plasma sprayed, functionally graded tungsten/steel coatings after process upscaling, Mater. Chem. Phys. 311 (2024) 128530, https://doi.org/10.1016/j.matchemphys.2023.128530.

[9] R. Vaßen, K.-H. Rauwald, O. Guillon, J. Aktaa, T. Weber, H.C. Back, D. Qu, J. Gibmeier, Vacuum plasma spraying of functionally graded tungsten/EUROFER97 coatings for fusion applications, Fusion Engineering and Design 133 (2018) 148–156, https://doi.org/10.1016/j.fusengdes.2018.06.006.

[10] D.D. Qu, W.W. Basuki, J. Gibmeier, R. Vaßen, J. Aktaa, Development of Functionally Graded Tungsten/EUROFER Coating System for First Wall Application, Fusion Science and Technology 68 (2015) 578–581. https://doi.org/10.13182/FST15-113.

[11] T. Weber, J. Aktaa, Numerical assessment of functionally graded tungsten/steel joints for divertor applications, Fusion Engineering and Design 86 (2011) 220–226, https://doi.org/10.1016/j.fusengdes.2010.12.084.

[12] D.D. Qu, W.W. Basuki, J. Aktaa, Numerical assessment of functionally graded tungsten/EUROFER coating system for first wall applications, Fusion Engineering and Design 98–99 (2015) 1389–1393, https://doi.org/10.1016/j.fusengdes.2015.06.120.

[13] X. Wang, M. He, Z. Guo, F. Wang, D. Zhou, Z. Wu, J. Huang, Preliminary studies on the main characteristics and transient heat shock performances of detonation sprayed tungsten coatings on 316 L steel substrates, Surf. Coat. Technol. 429 (2022) 127946, https://doi.org/10.1016/j.surfcoat.2021.127946.

[14] J. Klecka, J. Cizek, J. Matejicek, F. Lukac, J. Vala, Thick functionally-graded W-316L composite coatings for nuclear fusion applications, Nuclear Materials and Energy 34 (2023) 101373, https://doi.org/10.1016/j.nme.2023.101373.

[15] S. Heuer, J. Matějíček, M. Vilémová, M. Koller, K. Illkova, J. Veverka, Th. Weber, G. Pintsuk, J.W. Coenen, Ch. Linsmeier, Atmospheric plasma spraying of functionally graded steel/tungsten layers for the first wall of future fusion reactors, Surf. Coat. Technol. 366 (2019) 170–178, https://doi.org/10.1016/j.surfcoat.2019.03.017.

[16] G. Dose, S. Roccella, F. Romanelli, Engineering of a FGM Interlayer to Reduce the Thermal Stresses Inside the PFCs, Applied Sciences 12 (2022) 10215, https://doi.org/10.3390/app122010215.

[17] S. Heuer, Th. Weber, G. Pintsuk, J.W. Coenen, J. Matejicek, Ch. Linsmeier, Aiming at understanding thermo-mechanical loads in the first wall of DEMO: Stress–strain evolution in a Eurofer-tungsten test component featuring a functionally graded interlayer, Fusion Engineering and Design 135 (2018) 141–153, https://doi.org/10.1016/j.fusengdes.2018.07.011.

[18] S. Heuer, J.W. Coenen, G. Pintsuk, J. Matějíček, M. Vilémová, C. Linsmeier, Overview of challenges and developments in joining tungsten and steel for future fusion reactors, Phys. Scr. T171 (2020) 014028, https://doi.org/10.1088/1402-4896/ab47a4.

[19] E. Gaganidze, Material Property Handbook Tungsten, EUROfusion Internal Document IDM2P3SPL, 2020.

[20] S. Adachi, GaAs, AlAs, and $Al_xGa_{1-x}As$: Material parameters for use in research and device applications, J. Appl. Phys. 58 (1985) R1–R29, https://doi.org/10.1063/1.336070.

[21] G. Thomas, R. Vincent, G. Matthews, B. Dance, P.S. Grant, Interface topography and residual stress distributions in W coatings for fusion armour applications, Materials Science and Engineering: A 477 (2008) 35–42, https://doi.org/10.1016/j.msea.2007.05.120.

[22] A.K. Mishra, T. Grammes, J. Aktaa, Development of novel castellated functionally graded W/EUROFER coatings for fusion application, Mater. Des. 260 (2025) 115212, https://doi.org/10.1016/j.matdes.2025.115212.

[23] Y. Li, D. Zhu, C. He, Z. Guo, Y. Wang, C. Xuan, B. Wang, J. Chen, EAST Team, Thermomechanical analysis for the theoretical optimization of W/Cu monoblocks with functionally graded interlayer, Nuclear Materials and Energy 43 (2025) 101919, https://doi.org/10.1016/j.nme.2025.101919.

[24] K.A. Khor, Y.W. Gu, Effects of residual stress on the performance of plasma sprayed functionally graded ZrO2/NiCoCrAlY coatings, Materials Science and Engineering: A 277 (2000) 64–76, https://doi.org/10.1016/S0921-5093(99)00565-1.

[25] X.C. Zhang, B.S. Xu, H.D. Wang, Y. Jiang, Y.X. Wu, Modeling of thermal residual stresses in multilayer coatings with graded properties and compositions, Thin Solid Films 497 (2006) 223–231, https://doi.org/10.1016/j.tsf.2005.09.184.

[26] G. Schmidtmann, Y.J. Sohn, A. Litnovsky, M. Rasinski, R. Vaßen, J.W. Coenen, S. Brezinsek, Ch. Linsmeier, O. Guillon, G. Mauer, Optimizing Plasma Spraying Process Parameters for Tungsten Coatings Used in Fusion Reactors, Journal of Thermal Spray Technology 34 (2025) 2129–2144, https://doi.org/10.1007/s11666-025-02034-z.